Proceedings World Geothermal Congress 2020+1
Reykjavik, Iceland, April - October 2021

Observation of a Repeated Step-wise Fracture Growth During Hydraulic Fracturing Experiment at the Grimsel Test Site

Nathan Dutler*[a], Benoît Valley*, Linus Villiger**, Valentin Gischig*** and Florian Amann****

*Centre for Hydrogeology and Geothermics, University of Neuchâtel, Neuchâtel, Switzerland
**Swiss Seismological Service, ETH Zurich, Zurich, Switzerland
*** CSD Engineers, Bern, Switzerland
**** Department of Engineering Geology and Hydrogeology, RWTH Aachen, Aachen, Germany

[a] nathan.dutler@unine.ch

Keywords: hydraulic stimulation, reservoir mechanics, seismo-hydromechanical processes, stick-split mechanism, hydraulic clapping mechanism

ABSTRACT

Hydraulic fracturing (HF) experiments were conducted at the Grimsel Test Site (GTS), Switzerland, with the aim to improve our understanding of the seismo-hydro-mechanical processes associated with high-pressure fluid injection in a moderately fractured crystalline rock mass. Observations from one of these HF experiments indicate simultaneous propagation of multiple fractures during continuous fluid injection. The pressure measured in one observation interval show a cyclic response indicating repeated step-wise fracture growth. This is interpreted as a stick-split mechanism propagating fractures in an episodic manner and connecting them to the natural fracture network. In addition, transient partial closure and opening of fractures on the time-scale of seconds to minutes were observed from pressure and deformation monitoring. Our data set provides unprecedented insight in the complexity of hydraulic fracture propagation.

1. INTRODUCTION

Hydraulic fracturing is often used in reservoir engineering for shale gas/oil extraction and deep geothermal heat exploitation to increase the reservoir permeability and connectivity (Economides & Nolte, 2000; Evans et al., 2005). For deep enhanced geothermal systems (EGS), two prevalent concepts can be distinguished 1) hydraulic fracturing (HF) as the initiation and propagation of tensile fractures and 2) hydraulic shearing (HS) as the reactivation of pre-existing fractures in shear associated with dilation. These are end-members and a combination is possible i.e. primary fracturing with shear stimulation through leak-off or mixed-mechanism stimulation (McClure & Horne, 2014). The concepts for hydraulic fracturing for shale gas/oil extraction is generally similar but the objectives are different. For shale gas, establishing drainage of the formation from the production well is usually sufficient, while for an EGS a circulation between two or more boreholes need to be established. This is the crucial key process that depends on the target rock, the associated pre-existing fracture network, the temperature gradient and the stress field.

Current mathematical hydraulic fracture propagation models generally assume a single and continuous fracture growth (Adachi et al., 2007; Detournay, 2016). This kind of models simplify the complex nature of fracture propagation in-situ and are only valid in the context of single fracture propagation. Our experimental data sets challenge these simple assumptions as they show 1) multiple fracture growth and 2) intermittent fracture growth. Indeed, in low permeable rock mass with a pre-existing fracture network, the newly created hydraulic fracture will connect to the natural fracture network after a certain injection time (Dutler et al., 2019). This multi fracture extension mechanism is presented and discussed in this paper using the hydromechanical dataset from a hydraulic fracturing experiment. Concerning continuous fracture growth, a necessary condition is that the fluid flow speed at the crack tip matches the fracture propagation velocity. This interpretation is supported by the roughly constant fracture pressure propagation level (Zoback, 2007), which can be interpreted as continuous fracture growth by the absence of cyclic pressure fluctuation. Abundant geological evidence exist from outcrops that tensile fractures can growth in both continuous and episodic mode (Bahat & Engelder, 1984; Lacazette & Engelder, 1992). Van der Baan et al. (2016) proposed a new fracture growth mechanism during anthropogenic fluid injection, which is described in the following section.

Repeated brittle failure leads to microseismic events during hydraulic fracturing treatments (Cipolla et al, 2011; van der Baan et al, 2013). This repeated step-wise fracture growth is called **stick-split mechanism** proposed by van der Baan et al. (2016). The model assumes that the fracture propagation is driven by tensile failure at the tip. The fluid pressure has to sufficiently high so that the critical tensile fracture toughness value is exceeded. If local failure occurs the fracture extends and the fracture volume suddenly increases allowing fluid flow towards the new fracture tip. Therefore, a temporal local fluid pressure drop near the fracture tip can be observed so that the fracture partially closes there, until the fluid pressure builds up again due to continuous fluid injection. The repetition of these cycles leads to repeated step-wise fracture propagation.

The repeated episodes of abrupt local opening of the hydraulic fracture walls, followed by partial closing is called **hydraulic clapping mechanism.** It occurs during the stick-split mechanism after pressure drop following tensile propagation. Seismic evidence from this short opening and closing cannot be observed directly due to the characteristic time of the clapping effect, which is estimated to be around milliseconds. Therefore, the modulation in the source spectrum was used (Eaton et al., 2014; Walter & Brune, 1993). Transient pressure analysis from geothermal well tests indicate that a closed fracture near the wellbore after shut-in results in a buildup of pressure in the remaining part of the fracture in contact. This can result in a partial re-opening of the fracture to allow fluid flow towards the open borehole interval driven by the pressure difference (Bakar & Zarrouk, 2018; Zarrouk & McLean, 2019).

In this study, we present seismo-hydromechanical observations from a HF experiment (Dutler et al., 2019) providing evidence of the aforementioned fracturing mechanisms. The experiment is part of the In-situ stimulation and circulation project (Amann et al., 2018). The observations are discussed in term of 1) multiple fracture extension, 2) step-wise fracture growth and 3) hydraulic clapping mechanism.

2. STUDY SITE CHARACTERIZATION AND MONITORING

The study site is located in the Central Alps of Switzerland, below (~450 m) the Western flank of the Haslital valley in the southern part of the Grimsel Test Site. Prior to the hydraulic stimulation experiments, the rock mass of interest was characterized in great detail with respect to geology (Krietsch et al., 2018), geophysics (J Doetsch et al., 2017), stress field (Gischig et al., 2018; Krietsch et al., 2019) and hydrogeology (Brixel et al., 2019; Jalali et al., 2018).

The host rock consists of a moderately fractured and alpine overprinted granodiorite. Two sets of shear zones intersect the volume of interest. One set (S1.0, S1.1, S1.2 and S1.3) include four ductile shear zones characterized by a strong increase in the degree of foliation with an ENE-WSW strike and dip towards SSE. The most important shear zone is S1.0 next to the injection location (highlighted in Figure 1a). It experienced retrograde brittle deformation and contain a prominent discrete brittle fracture. The other set (S3.1 and S3.2) contains two brittle-ductile shear zones coinciding with two biotite-rich meta-basic dykes with an E-W strike and dip towards S. These bound a densely fractured zone with 10 fractures per meter. The most prominent feature is the brittle-ductile S3.1 shear zone, which is intersected by S1.0 and show prominent brittle fractures for flow transport towards the AU-tunnel. Two fracture systems are associated with the densely fractured zone in between the two meta-basic dykes of the brittle-ductile shear zone S3, where one system is sub-vertical and strike towards E-W and the other system sub-vertically strikes in N-S direction

The stress field has present strike-slip to thrust faulting conditions with a major principal stress axis towards E and dip of 40°. The magnitude of minimum and maximum principal stress is 8.6 MPa and 14.4 MPa, respectively. Approaching the brittle-ductile S3.1 shear zone from N, the stress field changes with a strike slip component, where the stress field is 30° rotated clockwise and intermediate and minimum principal stress axis switch place and the minimum principal stress magnitude reduces to 5.0 MPa (Dutler et al., n.d.; Krietsch et al., 2019).

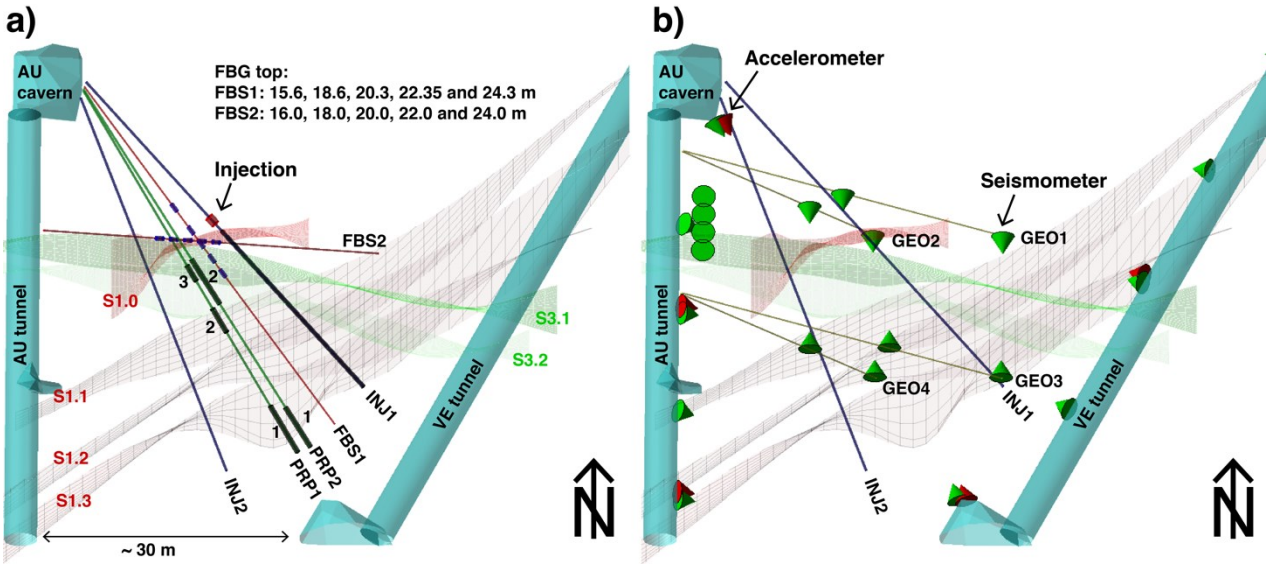

Figure 1: a) and b) Present the Geological Model with AU- and VE-tunnels, AU Cavern and Brittle-ductile Shear-zone S3 and Ductile Shear Zone S1. The Injection Location, the FBG Sensors in Borehole FBS1 and FBS2 and the Fracture Pressure Intervals in PRP1 and PRP2 are Presented in a). b) The Green and Red Cones Indicate the Location of the Installed Seismometers and Accelerometers, respectively.

In this paper, we present the results from one of a series of six HF injection experiments. This is the tests referred as HF3 in the experimental report and other publications (Doetsch et al., 2018; Dutler et al., 2019).The HF test was performed at the 16. May 2017 in the inclined borehole INJ1 using a 1 m long injection interval. The injection interval was placed from 19.8 to 20.8 m in the borehole INJ1, which was slightly north of the shear zone S1.0. Prior to stimulation this interval was free of visible discontinuities and transmissivity was in the order of 10^{-13} m^2/s indicating intact rock mass. During stimulation, injection pressure and flow rate were measured at the injection point. The fracture fluid pressure was also measured in the monitoring boreholes PRP1, PRP2 and INJ2. For the presented HF injection, data from intervals PRP1-2, PRP1-3 and PRP2-2 located in the brittle-ductile shear zone S3 are presented (location indicated as black cylinders in Figure 1a). 20 Fiber-Bragg Grating (FBG) sensors recording longitudinal deformation were installed in three boreholes (labelled FBS); we present 6 deformation time series from around the injection location (blue cylinders in Figure 1a). In addition, the time-strain plot from the Distributed Brillouin Strain Sensing (DSS) is presented for the sensor deployed along the PRP1 to track hydraulic connections. Positive strain indicate compression. The seismic monitoring network consists of total 26 uncalibrated piezo-electric acoustic emission (AE) sensors (green cones in Figure 1b) and 5 calibrated accelerometers (red cones). Eight AE sensors were installed in 4 geophysical boreholes (GEO) in close proximity to the injection interval (3-25 m).

3. RESULTS

The injection protocol of the HF experiment consists of three different cycles. The first injection cycle (F) aims to break down the formation and to initialize a new tensile crack. The two refracturing phases (RF1 and RF2) aim to propagate the fracture further into the pre-existing fracture network. The last cycle is a pressure-controlled step test (SR) to quantify final interval injectivity and jacking pressure based on the relationship of injection pressure and flow rate. The injection fluid was water and fracturing / refracturing are rate controlled cycles (Figure 2c, top). In the following, we will mainly focus on the first refracturing cycle.

3.1 Hydraulic Observations

The highest-pressure magnitude is observed during the breakdown cycle with a breakdown pressure of 16.3 MPa. The refracturing cycle RF1 reaches a maximum pressure of 8.3 MPa. With further fracture propagation the injection pressure stays below this maximum pressure. We observe a pressure limiting behavior at 6.8 MPa during cycle RF1 and RF2 for rates between 20 and 50 l/min. From the SR test, the final injectivity is 0.882 l/min/MPa and the jacking pressure is 5.1 MPa. The near wellbore transmissivity has increased to around 10^{-10} m^2/s.

During the first refracturing cycle RF1, a small pressure signal starts to form (up to 0.35 MPa, see Fig. 2d) in the observation pressure intervals (PRP1-2 and PRP2-2 at 12.3 and 4.9 m from the injection point). At 1500 s, the PRP1-3 respond with a repeated pressure increase and drop. The first pressure increase is almost instantaneous and reaches a maximum pressure of 1.4 MPa until pressure drops. This cycle lasts for 56 s, until the repetition starts with an increase in pressure reaching a magnitude of 1.6 MPa. This cycle lasts for 87 s and show an erratic pressure increase and drop with small amplitude at the end of the larger cycle, before it drops to a value of 0.6 MPa until shut-in. During shut-in time we observe two more pressure increase and drop with highest peak pressure of 2.2 respective 2.9 MPa (66% of injection pressure). The cycles are shorter and lasts for 25 respective 50 s (Fig. 2d).

The selected observation pressure intervals indicate an increase in pressure during refracturing cycle RF2. The pressure signal reaches its peak pressure of 1.6 MPa in PRP1-3, 3 s after shut-in. PRP2-2 reaches a peak pressure of 1.1 MPa with a delay time of 51 s and PRP1-2 reach the smallest peak pressure of 0.8 MPa, with the longest delay time of 156 s after shut-in. Note, that PRP1-3 respond to each flow step with a change in slope, where the other two observation points only show a gradual increase during injection. Minor transient changes (<0.1 MPa) are related to the pressure step test (Fig. 2c).

3.2 Mechanical Observations

The six longitudinal FBG strain sensors located in borehole FBS1 and FBS2 cover the shortest radial distance (2.8 – 6.3 m) to the injection interval (Fig. 2 a + b). The selected data traces show either only extensional (at borehole depths of 18.6, 20.4, 22.35, 20 m) or mixed (22.0, 24.0 m) strain (Fig. 2 c). The peak strain measures 863.5 με (during RF2 at 20 m). The same sensor responds by tension during the fracturing cycle, indicating a direct connection between injection interval and fracture intersecting the FBG sensor. Note that during RF1, the two sensors (at 22.35 and 20 m) with maximum tensional signal show direct response to the flow step during RF1 (Fig. 2 d).

The FBG sensor in FBS1 at 20.4 m reacts in compression during refracturing cycle RF1 (Fig. 2 d). The same sensor shows a compressional peak at 1217 s and reverse afterwards. The sensor next to it (18.6 m) shows a slight tensional reaction before reaching the peak tensional state, which is delayed (1237 s) compared with the sensor at 20.4 m. The FBG sensor at 24.3 m (in FBS1) show first a slight tensional signal and reverses at 1230 s and starts to be dominated by compression after 1282 s. At 1482 s, the sensor at 22.0 m (in FBS2) reaches a compressive peak and starts to reverse reaching a maximum change of -2.2 με/s. The sensor next to it (at 24.0 m) reaches the compressive peak at 1498 s and signals reverse as well, thereafter. The sensor at 20.0 m show peak tension of 713 με at 1490 s. Then, it starts to slightly reverse until shut-in (623 με). The sensors at 22.0 and 24.0 m show a delayed tensional peak after pump shut-in (1639 s) at 1668 s and 1707 s for the sensor at 22.0 m respective 24.0 m. The other sensors presented in Fig. 2 d do not show delayed peaks after pump shut-in.

The Distributed Brillouin Strain Sensing in borehole FBS1 (Fig. 2 c) indicate two fractures intersecting at 20.0 (1268 s) and 17.9 m (1772 s). The temporal sampling is limited to 126 s. Thus, the interpretation of the precise timing of fracture formation is limited. The fracture at 20.0 m is related to the S1.0 brittle overprinted shear-zone. The fracture at 17.9 m is a new hydraulic fracture supported by the observations that the next observed pre-existing fractures are at 16.8 or 18.4 m.

3.3 Seismic Response

In total, 79 events were localized during this HF experiment. 77 events (97.5%) occur during fluid injection and only 2.5% during pump shut-off. The amplitude magnitude of the events range between -3.1 and -4.9 (Villiger et al., n.d.). The event locations show a dispersed seismic pattern possibly related to the reactivation of two differently oriented fracture systems. The maximum radial distance between the injection interval and the seismic event observed is 15 m, where only two events have a bigger radial distance then 10 m.

26 events were localized during refracturing cycle RF1. Some events are located next to the boreholes and could possibly associated with the following effects: direct borehole effects including stress concentration, local change of pore water pressure, or compliance difference of concrete - rock mass and packer - rock mass. Another part is located in the targeted volume and show a dispersed pattern. The two fracture systems related with the S3 zone can probably explain this dispersed seismic pattern.

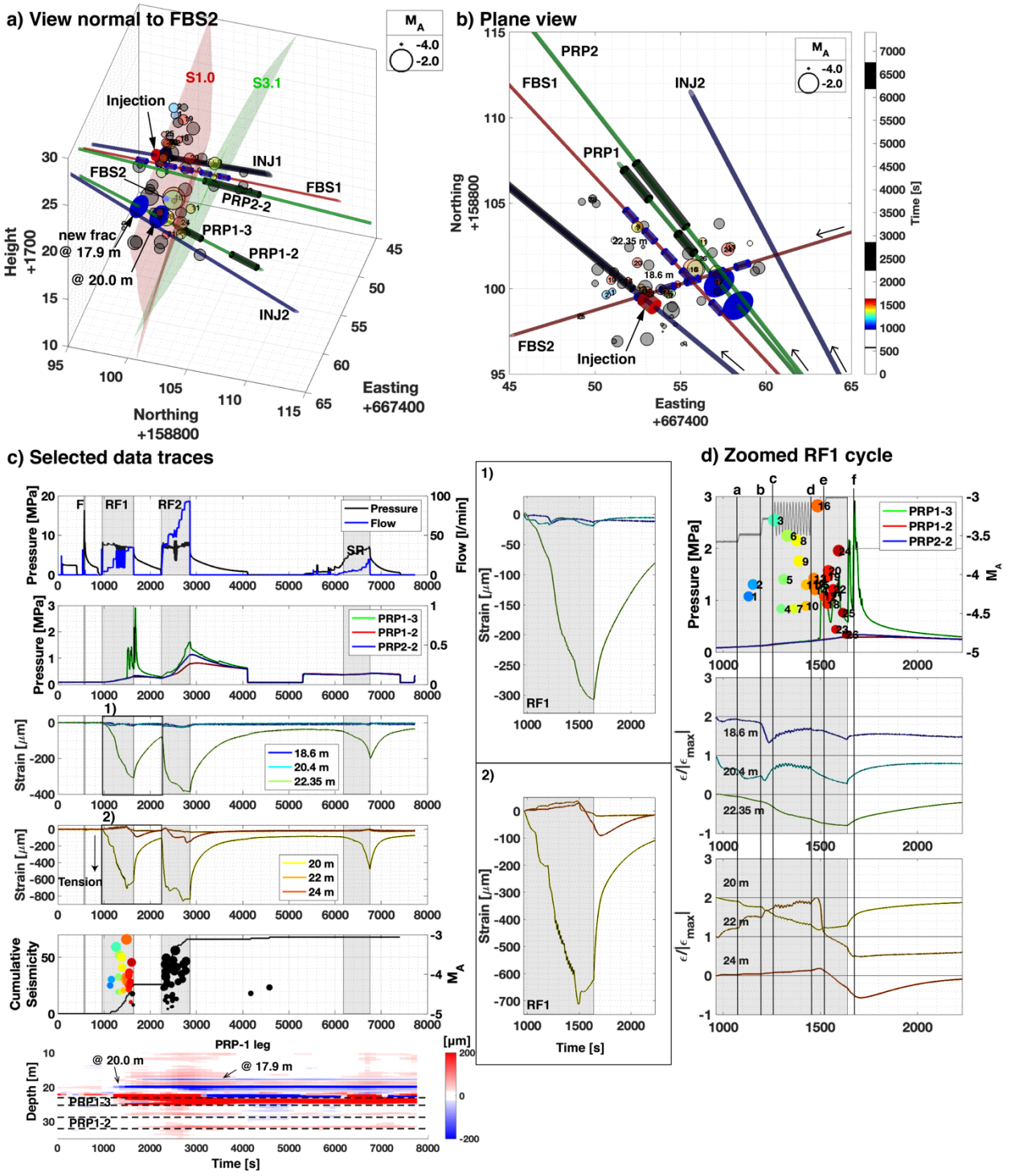

Figure 2: a) View normal to FBS2 inclusive S1.0 and S3.1 shear zone, boreholes, observation intervals and located seismic events (incl. color code) and fractures (blue ellipse); b) Plane view without shear zones; The black arrows indicate the plunge of the boreholes. c) Injection protocol; Timeseries of fracture fluid pressure interval PRP1-3, PRP1-2 and PRP2-2; Timeseries of strain multiplied (by the base length 1 m) data from the FBG sensors installed in FBS1 and FBS2; Amplitude magnitude of seismic events (highlighted for cycle RF1) and cumulative seismic; Timeseries of the Distributed Brillouin Strain Sensing (DSS) in PRP1 between 10 and 35 m borehole depth incl. highlighted PRP1-2 and PRP1-3 interval; d) Zoomed RF1 cycle for the transient pressure, seismic amplitude magnitude (incl. numbers) and strain curves. The numbers and color code of the seismic events correspond to the same numbers and color in a) and b). The flow rate is indicated in grey scaled between 2 and 3 MPa for 0 to 35 l/min.

4. DISCUSSION SEISMO-HYDROMECHANICS

4.1 Multiple Fracture Extension

We demonstrate multiple fracture extension by following the timeseries in Fig. 2d and show three snapshots of the deformation labelled from a to f (Fig. 2d) and the corresponding seismic events (Fig. 3). Between time b and c, we observe two FBG sensors (18.6 and 20.4 m) which first show tensional increase and reverse during cyclic injection before the flow rate is ramped up. It seems that both sensors react to the dominant signal observed at 22.35 m, which first show compression and reverse to tension. This can be interpreted as the arriving fracture and fluid front, which reaches first the sensor at 18.6 m, then the one at 20.4 m and starts to open the fracture intersecting the base length of the sensor at 22.35 m. Note that the position of these fracture openings does not align with the predominant E-W striking seismicity cloud interpreted as the main hydraulic fracture orientation. Thus, we argue that not a single fracture, but multiple strands of fractures propagate to through rock mass. This compressive front before the fluid arrives increases with injection volume and can be associated with the poro-elastic effect produced by the pressurized fluid-rock volume. In addition, the Distributed Brillouin Strain Sensing in FBS1 show a tensional signal at 20.0 m (lower blue circle in Fig. 3) at the same time. The tensional signal does not go back to zero at the end of the experiment indicating a mismatch between the two fracture planes due to a shear component.

At the time d (Fig. 3), two FBG sensor (FBS1 at 22.35 m and FBS2 20.0 m) show abrupt tensional responses with reaching tensile strain of 386 and 862 microstrain, respective. The FBG sensor at 22.35 in FBS1 covers factures associated with S3.1 zone. Since both sensors respond in a similar way, it has to connected with the fractures intersecting the FBG sensor at 20 m in FBS2 (biggest tensional response). Also, the PRP1 observation at 20.0 m (blue circle in Fig. 3) indicates connectivity to the same fracture system. showing continuously increasing pressure. Six of nine seismic events are located next to the sensors described before. The new fracture trace in the injection interval is presented by the blue disc (Fig 2a).

Table 1: Overview of the Monitoring System Response Including Number of Fractures in the Monitoring Interval (Prior to Stimulation), Related Fracture System and Maximum Pressure or Respectively FBG Measurement Magnitude During Refracturing Cycle RF1.

Depth [m]	Borehole	Monitoring system	No. of fractures	Fracture system	Maximum Pressure [MPa] / FBG measurement [μm] during RF1
19.8-20.8	INJ1	HF3 Injection location	0	-	8.3 MPa
27.2-28.2	INJ1	HS4 Injection location	3	S3.1	-
22.0-23.0	INJ1	HS8 Injection location	2	S1.0	-
28.9-32.0	PRP12	Fracture pressure	5	S3.2	0.3 MPa
23.2-25.2	PRP13	Fracture pressure	5	S3.1	2.9 MPa
21.4-27.0	PRP22	Fracture pressure	11	S3.1/S3.2	0.3 MPa
18.6-19.6	FBS1	FBG	0	-	-22.3 μm
20.4-21.4	FBS1	FBG	0	S1.0	-26.7 μm
22.35-23.35	FBS1	FBG	1	S3.1	-386.1 μm
20.0-21.0	FBS2	FBG	2	-	-863.5 μm
22.0-23.0	FBS2	FBG	0	-	33.7 μm
24.0-25.0	FBS2	FBG	0	-	-158.9 μm

The FBG sensor at 20 m indicates fluid flow through the intersecting fractures due to direct strain change with each flow rate step increase (Fig. 2c). From time d to e, the sensor at 22 and 24 m first show compression and start to reverse until tensional signals are observed, indicating existing fractures (Fig. 2d). The number of fractures intersecting the base length of the FBG sensor (Table 1) increases if new hydraulic fractures or sealed fractures are connected to the injection interval. Especially FBG sensors in intact rock (no intersecting natural fractures) should only show compression next to the injection location. Prior to the HF stimulation the HS stimulation took place. The HS4 injection stimulated the S3.1 zone. A strong instantaneous tensional signal was observed the FBG sensor in FBS2 at 24.0 m indicating that a new hydraulic fracture towards this sensor has been formed. The same fracture at this FBG sensor was reactivated during stimulation HS8 targeting the zone S1.0. During refracturing cycle RF1 from HF3, three FBG sensors (at 20, 22 and 24 m in FBS2), changed their behavior ~2 s prior to the instantaneous pressure increase in the PRP1-3. These changes can be recognized in the snapshot at time e (Fig. 3), 1) the bigger magnitude of pressure in PRP1-3 can be observed, 2) the FBG sensor at 22.0 m in FBS2 reverse (green->white) and 3) more seismic events are located, where the new events occur at the same patches similar to time d.

The snapshot at time f (Fig. 3) during pump shut–in time show only small changes compared to the snapshot at time e. 1) The magnitude for the interval PRP1-3 reaches its maximum, and 2) the strain sensor at 24 m in FBS2 is now tensional. The new seismic events occurring during Time e and Time f are located next to the previous events (grouped with black circles in Fig. 3). Strain measured with Distributed Brillouin Strain Sensing in FBS1 starts showing a tensional signal at 17.9 m during this pump shut-off time. We assume that a new hydraulic connection is formed related to the fracturing processes around PRP1-3 at the end of RF1 and shut-in time. The FBG sensors at 22 and 24 m show an unusual long delay time between shut-in and reaching tensional peak (Fig. 2d). The fluid path ways being blocked towards the injection borehole due to mechanical effects. Thus, fluid is pushed further into the reservoir resulting in delayed pressure peaks.

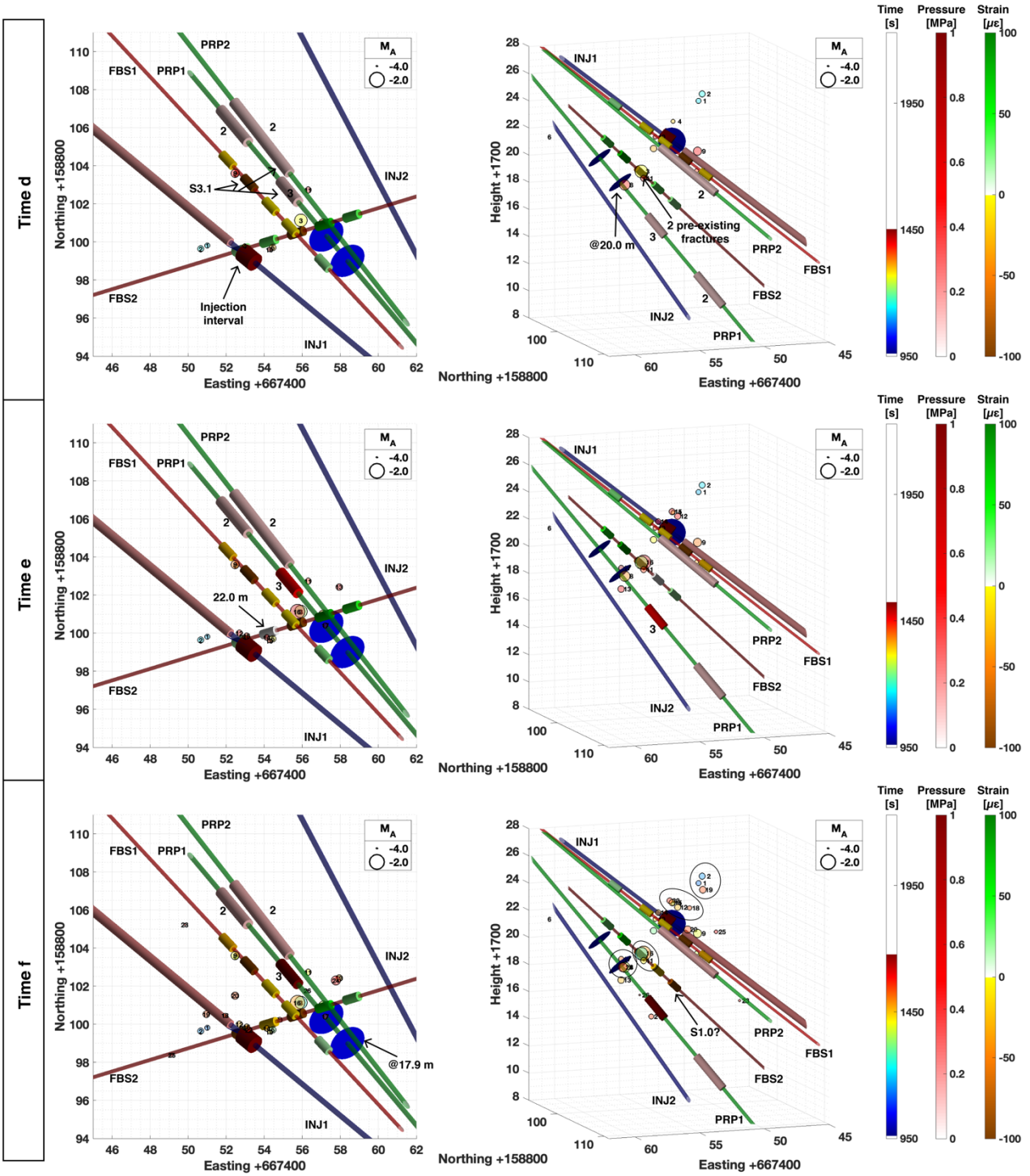

Figure 3: Seismo-hydromechanical Observations Visualized Looking on Plane View (Left Column) and Parallel to the Shear Zones (Right Column). Each Row Represents a Temporal Resolved Snapshot at time d, e and f Presented in Figure 2d.

The cubic law in its simplest form ($T = a^3/12$) can be used to convert potential fracture opening measured with FBG sensors (a) into transmissivity (T). Assuming a single fracture has an initial aperture of 10 µm, then the transmissivity is in the order of 10^{-17} m^3. The largest observed tensional FBG measurement during the first refracturing cycle is 863.5 µm and leads to a transmissivity of 10^{-11} m^3. The local transmissivity change in the volume is at least in the order of 6 magnitudes.

4.2 Stick-split Mechanism

The schematic representation of the stick-split mechanism (Fig. 4a) is used to interpret the pressure observations in PRP1-3 (Figure 4b). The process can be divided in four stages. 1) The fluid pressure builds up and the aperture near the tip increases (stick). 2) The effective pressure exceeds the tensile strength of the rock and local failure occurs (split). The abrupt increase in volume due to fracture extension allows the fluid to flow towards the new fracture tip location. 3) The volume increase is accompanied by a local and temporal pressure drop some distance from the fracture tip. Therefore, the fracture partially closes there. 4) Then, pressure start to build up again with continuous injection until a new stick-split cycle starts.

During refracturing cycle RF1, we observed a cyclic variation in the fracture pressure interval PRP1-3. We relate the different stages from the stick-split mechanism with the pressure observation (Fig. 4b) described in section 3.1. The change in pressure is not related to changes in the flow rate in the injection borehole (except at 1525s). For conceptualization let us assume a parallel plate approximation with a laminar flow through it. This problem depends entirely on fluid velocity, pressure gradient, fluid viscosity and plate aperture. Assuming a constant viscosity and a given aperture leads to a correlation between fluid velocity (flow rate) and pressure gradient. However, the presented pressure observation from PRP1-3 and the injection rate contradicts this. We know from lab tests that the tensile strength of intact Grimsel Gneiss is at least 5.6 MPa (Dutler et al., 2018). The time scale mentioned by Van Der Baan et al. (2016) between opening and partial closing at the tip is in milliseconds. The pressure curve indicates different time scale with times of 56 and 87 s for a cycle. We explain this by the fact that the fracture is not initially created in intact rock and the volume to be filled is relatively big. Indeed, when of sealed fractures breaks and the fluid flow not only towards the new fracture tip but also to the associated new connected fracture volume and thus the time scale increases. It also dissipates the local pressure drop and the associated partial fracture closure near the fracture tip.

An alternate explanation for the pressure signal of Fig. 4b could be packer leakage. We can exclude this explanation because before we see the abrupt increase in PRP1-3, we see at 20 m a tensional signal in the Distributed Brillouin Strain Sensing. Therefore, we know that the water bearing fracture at 20 m is not changing the packer performance. We do see this cyclic change only during the refracturing cycle RF1 for experiment HF3. Cycle RF2 and all other experiments (especially the one performed later) do not indicate packer problems. Therefore, we assume these signals are in-situ evidence of the complex stick-split hydromechanical interaction and thus validate the existence of this process.

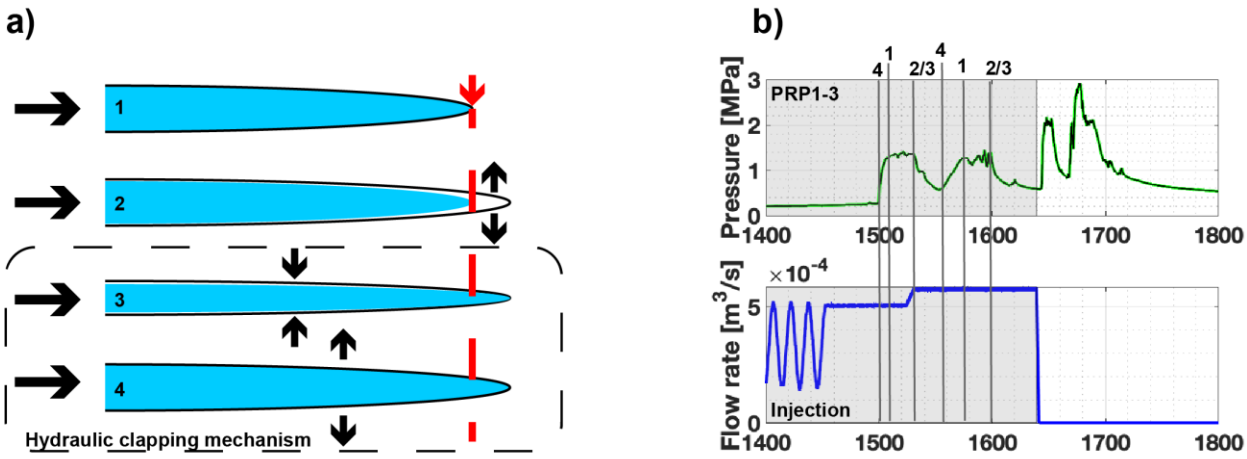

Figure 4: a) Schematic Representation of the Stick-split Mechanism in Four Stages Inclusive Hydraulic Clapping Mechanism (Last Two Stages) and b) Applying the Stages to the PRP1-3 Pressure Data from the HF3 Experiment Inclusive Injection Overview.

We interpret this in terms of the pressure diffusion equation that is based on coupling Darcy's law with the continuity equation:

$$\frac{\partial}{\partial x}\left(T_x \frac{\partial p}{\partial x}\right) + \frac{\partial}{\partial y}\left(T_y \frac{\partial p}{\partial y}\right) = \frac{1}{\rho_f}\left(S_f \frac{\partial p}{\partial t}\right) \quad (1)$$

where p is the fluid pressure, T_i is the transmissivity, ρ_f is the fluid density (constant) and S_f is the storage coefficient of the fracture. If we assume constant transmissivity, an increase in the flow-rate at the injection interval (source) leads to change in the head for a cell next to the injection location. This agrees with our observation that the progressively increasing injection leads to an increase in the observation pressure. Considering the cyclic change in pressure in the observation interval PRP1-3, a fracture propagating in a stick-split manner may affect pressure (or head) in three ways: 1) by a change in the pressure (or head) gradient due to a pressure drop at the propagation front, 2) a change in the storage coefficient due to continued fracture opening as well as the void space created by the fracture propagation , 3) change in fracture aperture leading to a change in transmissivity. The three effects may act in concert to produce cyclic pressure behind a propagating fracture.

4.3 Hydraulic Clapping Mechanism

The last two cycles of PRP1-3 (Fig. 4b) are most likely observations of the hydraulic clapping mechanism. These cycles occur during shut-in phase (pump is shut-off and injection line is closed), when fracture closure dominates.

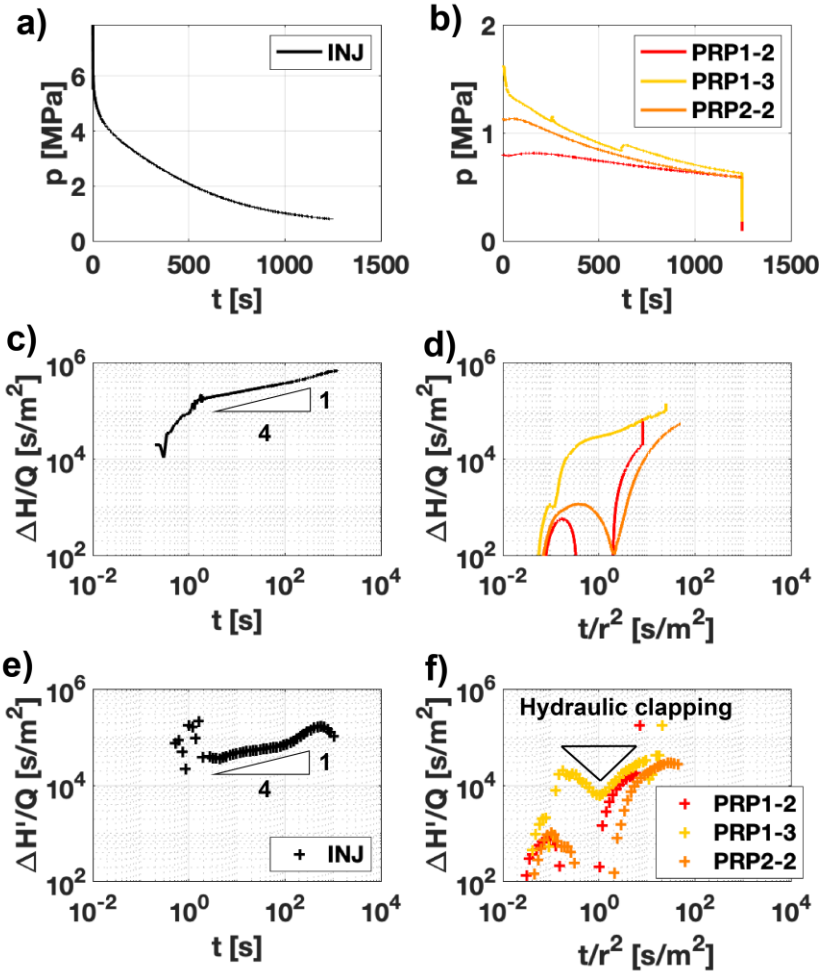

Figure 5: a+b) Timeseries of Shut-in time for RF2 from the Injection and Observation Pressure Intervals. Log-log Normalized Hydraulic Fracturing Response ($\Delta H/Q$) from the Drawdown of Refracturing Cycle RF2 and Bourdet Derivative ($\Delta H'/Q$) for c+e) the Injection Curve and d+f) the Observation Curves with Normalized Distance.

The normalized drawdown for the injection curve for refracturing cycle RF2 show a dominant bilinear flow regime (slope ¼ in both $\Delta H/Q$ and derivative in Fig. 5a). At late time (~ 600 s), the derivative reaches a peak, which can be interpreted as reaching a constant head boundary. We interpret this as fluid flow drained by the S3.1 or S1.0 towards the AU-tunnel. The drawdown observed in the monitoring intervals show strong pressure (head) variation for PRP1-2 and PRP2-2. Note that the time for the observation intervals is corrected by distance between the midpoint of the injection and observation intervals. The drawdown curve of PRP1-2 is slightly convex (~1 s). The derivative of all these curves show slight hump for PRP2-2 and strong humps for PRP1-2 and PRP1-3. Bakar & Zarrouk (2018) showed that these humps are related to hydraulic fracture clapping. The difference to their study is that we observe these signals not at the injection interval, but in the observation intervals. The hydraulic clapping is observed at around 1 s (triangle Fig. 5b), which is early compared with the observations of Bakar & Zarrouk (2018) at around 200 s for well test data from geothermal fields. It is an open question if our observation is also related to the poro-elastic wave driven by the instantaneous pressure loss in the injection interval.

4.4 Hydromechanical Interaction

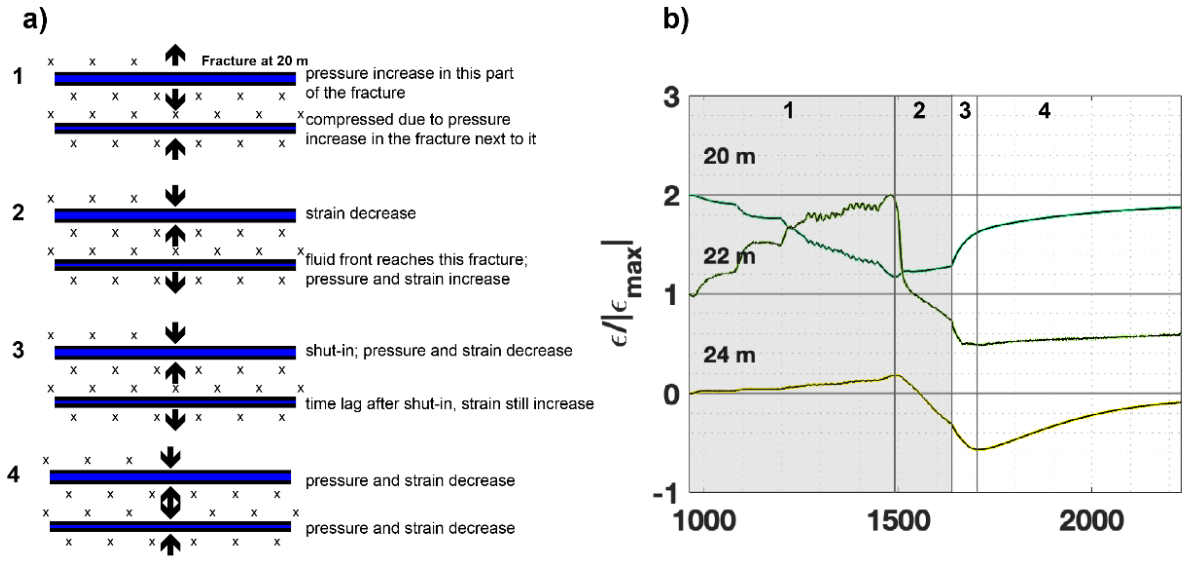

Figure 6: a) Scheme of a Multiple-fracture System Presented in b). The Zoomed RF1 Cycle for Three FBG Strain Curves from Borehole FBS2.

The observations from three FBG sensors at 20, 22 and 24 m in FBS2 presented in the result section are interpreted in Fig. 6. The hydromechanical interaction between two fractures can explain the observed strain curves. We divided the normalized strain time series in four stages. 1) The fracture at 20 m respond with an increasing aperture by increasing flow rate. The fracture at 22 and 24 m reacts with compression. 2) The aperture for the fracture at 20 m reaches its maximum and then slightly decrease. The fractures at 24 m react with strain increase. We assume that we created a new hydraulic connection towards these two fractures. 3) At shut-in, the aperture of the fracture at 20 m decrease. The other two fractures show a time lag reaching its maximum fracture aperture. The time lag observed is dependent on the distance and the connectivity from the injection borehole to this observation point, if we assume that these signals are related to fluid flow through the fractures. 4) After reaching the maximum fracture aperture, two of three FBG sensors indicate relaxation. The sensor at 22 m, indicate permanent strain change of -21.9 με and therefore simple fracture opening and closing cannot explain this signal. We relate this permanent change to hydraulic shearing with dilation along the pre-existing fractures intersecting the base length of this FBG sensor.

5. CONCLUSION

The presented hydromechanical data from one hydraulic fracturing experiment indicate complex mechanisms between continuous fluid injection, episodic fracture propagation, interaction and connection of hydrofractures with the natural fracture system. We highlighted different responses of the FBG sensors during the experiment and related it to local transmissivity increase. The observed fracture pressure increases along with the variable spatial and temporal occurrence of seismicity indicates the new hydraulic fractures propagates as multiple fracture branches that connect to the pre-existing fracture network. Observed fracture pressure in observation intervals with pre-existing fractures shows that rock mass stimulation occurs mainly through connecting pre-existing fractures and to a minor extend through the creation of new fractures in intact rock. Observed pressure indicate a non-uniform pressure distribution in the network during continuous fluid injection. Additionally, observed cyclic pressure observations during constant rate injection indicating an episodic fracture growth that is interpreted as stick-split mechanism breaking intact rock and connecting pre-existing fractures. We further observe post-shut-in pressure reversals during pressure decay. Normalized drawdown curves of these pressure decay curves may be interpreted as interaction of nearby fractures that close and open in response to spatially heterogeneous pressure diffusion to the far-field. Hydromechanical interaction between two fractures being formed and pressurized at different times is evident.

ACKNOLEDGMENTS

This study is part of the In-situ Stimulation and Circulation (ISC) project established by the Swiss Competence Center for Energy Research - Supply of Electricity (SCCER-SoE) with the support of Innosuisse. Funding for the ISC project was provided by the ETH Foundation with grants from Shell and EWZ and by the Swiss Federal Office of Energy through a P&D grant. Nathan Dutler is supported by SNF grant 200021_165677. The Grimsel Test Site is operated by Nagra, the National Cooperative for the Disposal of Radioactive Waste. We are indebted to Nagra for hosting the ISC experiment in their GTS facility and to the Nagra technical staff for onsite support.

REFERENCES

Adachi, J., Siebrits, E., Peirce, A., & Desroches, J. (2007). Computer simulation of hydraulic fractures. *International Journal of Rock Mechanics and Mining Sciences*, *44*(5), 739–757. https://doi.org/10.1016/j.ijrmms.2006.11.006

Amann, F., Gischig, V., Evans, K., Doetsch, J., Jalali, R., Valley, B., … Giardini, D. (2018). The seismo-hydromechanical behavior during deep geothermal reservoir stimulations: open questions tackled in a decameter-scale in situ stimulation experiment. *Solid Earth*, *9*(1), 115–137. https://doi.org/10.5194/se-9-115-2018

Bahat, D., & Engelder, T. (1984). Surface morphology on cross-fold joints of the Appalachian Plateau, New york and Pennsylvania. *Tectonophysics*. https://doi.org/10.1016/0040-1951(84)90128-8

Bakar, H. A., & Zarrouk, S. J. (2018). Transient pressure analysis of geothermal wells fractured during well testing. *Geothermics*, *76*(June 2017), 26–37. https://doi.org/10.1016/j.geothermics.2018.06.010

Brixel, B., Klepikova, M., Jalali, M., Roques, C., Lei, Q., Krietsch, H., & Loew, S. (2019). Emergence of anomalous diffusion in shear zones: Insights from in-situ forced flow experiments. *AGU Solid Earth*, (in review).

Cipolla, C. L., Mack, M. G., Maxwell, S. C., & Downie, R. C. (2011). A Practical Guide to Interpreting Microseismic Measurements, (June), 14–16. https://doi.org/10.2118/144067-ms

Der Baan, M. van, Eaton, D. W., & Preisig, G. (2016). Stick-split mechanism for anthropogenic fluid-induced tensile rock failure. *Geology*, *44*(7), 503–506. https://doi.org/10.1130/G37826.1

Detournay, E. (2016). Mechanics of Hydraulic Fractures. *Annual Review of Fluid Mechanics*, *48*(1), 311–339. https://doi.org/10.1146/annurev-fluid-010814-014736

Doetsch, J, Krietsch, H., Lajaunie, M., Schmelzbach, C., Maurer, H., & Amann, F. (2017). GPR imaging of shear zones in crystalline rock. In *Conference: 2017 9th International Workshop on Advanced Ground Penetrating Radar (IWAGPR)*. Retrieved from https://doi.org/10.1109/IWAGPR.2017.7996074

Doetsch, Joseph, Gischig, V., Krietsch, H., Villiger, L., Amann, F., Dutler, N., … Giardini, D. (2018). *Grimsel ISC Experiment Description*. Zurich. Retrieved from https://doi.org/10.3929/ethz-b-000310581

Dutler, N., Nejati, M., Valley, B., Amann, F., & Molinari, G. (2018). On the link between fracture toughness, tensile strength, and fracture process zone in anisotropic rocks. *Engineering Fracture Mechanics*, *201*, 56–79. https://doi.org/10.1016/j.engfracmech.2018.08.017

Dutler, N. O., Jalali, M., Gischig, V. S., Valley, B., Brixel, B., Roques, C., … Amann, F. (n.d.). Observation of fracture closure during in-situ hydraulic fracturing. *Energies*, in prep.

Dutler, N., Valley, B., Gischig, V., Villiger, L., Krietsch, H., Doetsch, J., … Amann, F. (2019). Hydraulic fracture propagation in a heterogeneous stress field in a crystalline rock mass. *Solid Earth Discussions*, 1–41. https://doi.org/10.5194/se-2019-111

Eaton, D. W., van der Baan, M., Birkelo, B., & Tary, J. B. (2014). Scaling relations and spectral characteristics of tensile microseisms: Evidence for opening/closing cracks during hydraulic fracturing. *Geophysical Journal International*, *196*(3), 1844–1857. https://doi.org/10.1093/gji/ggt498

Economides, M., & Nolte, K. (2000). *Reservoir Stimulation*. Chichester: Wiley. https://doi.org/10.1017/CBO9781107415324.004

Evans, K. F., Moriya, H., Niitsuma, H., Jones, R. H., Phillips, W. S., Genter, A., … Baria, R. (2005). Microseismicity and permeability enhancement of hydrogeologic structures during massive fluid injections into granite at 3 km depth at the Soultz HDR site. *Geophysical Journal International*, *160*(1), 388–412. https://doi.org/10.1111/j.1365-246X.2004.02474.x

Gischig, V. S., Doetsch, J., Maurer, H., Krietsch, H., Amann, F., Evans, K. F., … Giardini, D. (2018). On the link between stress field and small-scale hydraulic fracture growth in anisotropic rock derived from microseismicity. *Solid Earth*, *9*(1), 39–61. https://doi.org/10.5194/se-9-39-2018

Jalali, M., Klepikova, M., Doetsch, J., Krietsch, H., Brixel, B., Dutler, N. O., … Amann, F. (2018). A Multi-Scale Approach to Identify and Characterize the Preferential Flow Paths of a Fractured Crystalline Rock. In *2nd International DFNE Conference* (p. 0734). Seattle.

Krietsch, H., Doetsch, J., Dutler, N., Jalali, M., Gischig, V., Loew, S., & Amann, F. (2018). Comprehensive geological dataset describing a crystalline rock mass for hydraulic stimulation experiments. *Scientific Data*, *5*, 180269. https://doi.org/10.1038/sdata.2018.269

Krietsch, H., Gischig, V., Evans, K., Doetsch, J., Dutler, N. O., Valley, B., & Amann, F. (2019). Stress Measurements for an In Situ Stimulation Experiment in Crystalline Rock: Integration of Induced Seismicity, Stress Relief and Hydraulic Methods. *Rock Mechanics and Rock Engineering*, *52*(2), 517–542. https://doi.org/10.1007/s00603-018-1597-8

Lacazette, A., & Engelder, T. (1992). Fluid-driven Cyclic Propagation of a Joint in the Ithaca Siltstone, Appalachian Basin, New York. *International Geophysics*, *51*(C), 297–323. https://doi.org/10.1016/S0074-6142(08)62827-2

McClure, M. W., & Horne, R. N. (2014). An investigation of stimulation mechanisms in Enhanced Geothermal Systems. *International Journal of Rock Mechanics and Mining Sciences*, *72*, 242–260. https://doi.org/10.1016/j.ijrmms.2014.07.011

van der Baan, M., Eaton, D., & Dusseault, M. (2013). Microseismic Monitoring Developments in Hydraulic Fracture Stimulation. In A. Bunger, J. McLennan, & R. Jefrey (Eds.), *Effective and Sustainable Hydraulic Fracturing* (pp. 439–466). InTech. Retrieved from http://dx.doi.org/10.5772/56444

Villiger, L., Gischig, V. S., Doetsch, J., Selvadurai, A. P., Krietsch, H., Dutler, N. O., … Wiemer, S. (n.d.). On the variability of seismic response during multiple decameter-scale hydraulic stimulations in crystalline rock. *(In Prep)*.

Walter, W. R., & Brune, J. N. (1993). Spectra of seismic radiation from a tensile crack. *Journal of Geophysical Research*, *98*(B3), 4449–4459. https://doi.org/10.1029/92JB02414

Zarrouk, S. J., & McLean, K. (2019). *Geothermal Well Test Analysis*. (Elsevier, Ed.). London: Katie Hammon.

Zoback, M. D. (2007). *Reservoir Geomechanics*. https://doi.org/10.1017/CBO9780511586477